Physics Letters B 723 (2013) 71–77

Contents lists available at SciVerse ScienceDirect

Physics Letters B

www.elsevier.com/locate/physletb

First measurement of the helicity dependence of ^{3}He photoreactions in the $\Delta(1232)$ resonance region

P. Aguar Bartolomé [j], A. Mushkarenkov [o,1], J. Ahrens [j], J.R.M. Annand [g], H.-J. Arends [j], R. Beck [b], V. Bekrenev [e], H. Berghäuser [f], A. Braghieri [o], W.J. Briscoe [t], S.N. Cherepnya [n], S. Costanza [o], P. Drexler [f], L.V. Fil'kov [n], A. Fix [r], G. Giardina [l,c], D.I. Glazier [d], D. Hamilton [g], E. Heid [j], W. Heil [k], D. Hornidge [q], D. Howdle [g], I. Jaegle [a], O. Jahn [j,2], T. Jude [d,2], V.L. Kashevarov [j,n], I. Keshelashvili [a], R. Kondratiev [m], M. Korolija [u], J. Krimmer [k,3], B. Krusche [a], S. Kruglov [e], A. Kulbardis [e], V. Lisin [m], K. Livingston [g], J. Mancell [g], D.G. Middleton [j,q], I.J.D. MacGregor [g], D.M. Manley [h], J.C. McGeorge [g], V. Metag [f], B.M.K. Nefkens [i], A. Nikolaev [b], M. Oberle [a], M. Ostrick [j], H. Ortega [j], P.B. Otte [j], B. Oussena [j], P. Pedroni [o,*], F. Pheron [a], S. Prakhov [i], A. Polonski [m], F. Rigamonti [o,p], M. Romaniuk [l,c], G. Rosner [g], T. Rostomyan [a], S. Schumann [j], D. Sober [s], A. Starostin [i], I. Supek [u], M. Thiel [f], A. Thomas [j], M. Unverzagt [j], D. Watts [d], D. Werthmüller [a]

[a] *Institut für Physik, University of Basel, CH-4056 Basel, Switzerland*
[b] *Helmholtz-Institut für Strahlen und Kernphysik, University of Bonn, D-53115 Bonn, Germany*
[c] *INFN, Sezione di Catania, I-95123 Catania, Italy*
[d] *SUPA School of Physics & Astronomy, University of Edinburgh, Edinburgh EH9 3JZ, UK*
[e] *Petersburg Nuclear Physics Institute, RU-188300 Gatchina, Russia*
[f] *II Physikalisches Institut, University of Giessen, D-35392 Giessen, Germany*
[g] *SUPA School of Physics & Astronomy, University of Glasgow, Glasgow G12 8QQ, UK*
[h] *Kent State University, Kent, OH 44242-0001, USA*
[i] *University of California, Los Angeles, CA 90095-1547, USA*
[j] *Institut für Kernphysik, University of Mainz, D-55128 Mainz, Germany*
[k] *Institut für Physik, University of Mainz, D-55128 Mainz, Germany*
[l] *Dipartimento di Fisica e Scienze della Terra, Università di Messina, I-98166 Messina, Italy*
[m] *Institute for Nuclear Research, RU-125047 Moscow, Russia*
[n] *Lebedev Physical Institute, RU-119991 Moscow, Russia*
[o] *INFN, Sezione di Pavia, I-27100 Pavia, Italy*
[p] *Dipartimento di Fisica Nucleare e Teorica, Università di Pavia, I-27100 Pavia, Italy*
[q] *Mount Allison University, Sackville, NB, E4L 1E6, Canada*
[r] *Tomsk Polytechnic University, Tomsk, Russia*
[s] *The Catholic University of America, Washington, DC 20064, USA*
[t] *The George Washington University, Washington, DC 20052-0001, USA*
[u] *Rudjer Boskovic Institute, HR-10000 Zagreb, Croatia*

ARTICLE INFO

Article history:
Received 8 January 2013
Received in revised form 27 April 2013
Accepted 28 April 2013
Available online 3 May 2013
Editor: D.F. Geesaman

Keywords:
^{3}He photo-absorption
Polarisation observables
Nucleon spin structure

ABSTRACT

The first measurement of the helicity dependence of the total inclusive ^{3}He photo-absorption cross section and of the partial cross sections for several reaction channels was carried out at MAMI (Mainz) in the photon energy range between 150 and 500 MeV. The experiment used the large acceptance Crystal Ball spectrometer, complemented by charged particle and vertex detectors, a circularly polarised tagged photon beam and a longitudinally polarised high-pressure ^{3}He gas target. The results obtained give information on the GDH integral on ^{3}He and on the neutron and allow an investigation of the modifications of nucleon properties inside ^{3}He.

0370-2693/$ – see front matter © 2013 Published by Elsevier B.V.
http://dx.doi.org/10.1016/j.physletb.2013.04.057

1. Introduction

For many years an intensive experimental programme has been carried out with the principal aim to verify the well-known Gerasimov–Drell–Hearn (GDH) sum rule [1,2]. This sum rule relates the anomalous magnetic moment κ of a particle of spin S and mass M to the integral over the weighted helicity-dependent total absorption cross section difference for circularly polarized photons on a longitudinally polarized target:

$$I_{\mathrm{GDH}} = \int_{\nu_{th}}^{\infty} \frac{\sigma_p - \sigma_a}{\nu}\, d\nu = 4\pi^2\kappa^2 \frac{e^2}{M^2} S, \tag{1}$$

where σ_p and σ_a are the total absorption cross sections for parallel and antiparallel relative spin configurations, respectively, and the cross section is weighted by the inverse of the photon energy ν. The lower limit of the integral, ν_{th}, corresponds to the pion photoproduction (photodisintegration) threshold for a free-nucleon (nuclear) target. The GDH sum rule is derived from the very general physical principles of Lorentz and gauge invariance, causality, unitarity, and an unsubtracted dispersion relation applied to the forward scattering amplitude. A measurement of the GDH integral constitutes a fundamental check of these assumptions. The first experimental check of the GDH sum rule for the proton was carried out jointly at the Mainz and Bonn tagged photon facilities, where $I^{\mathrm{p}}_{\mathrm{GDH}}$ was experimentally evaluated in the photon energy range $0.2 < E_\gamma < 2.9$ GeV by the GDH Collaboration [3–5]. The combination of this result with the theoretical predictions for the unmeasured energy ranges supports the validity of the GDH sum rule for the proton.

An investigation of the isospin structure of the GDH sum rule requires additional measurements on the neutron. In this case the interpretation of the experimental data is more complicated: the lack of free neutron targets necessitates the use of neutrons bound in ^{2}H or ^{3}He. The first experimental measurement using longitudinally polarised deuterons was performed in the energy region between 0.2 and 1.8 GeV by the GDH Collaboration [6–8]. In [8] a very rough estimate was derived for the GDH integral value for the neutron from the combination of the measurements on the deuteron and the proton. However, a lack of reliable nuclear models for describing the helicity-dependent γ ^{2}H interactions in a satisfactory manner and the presence of a large proton background contribution currently prevent a reliable extraction of the GDH neutron value from measurements on ^{2}H targets.

A complementary and more direct access to a free polarised neutron is given by a longitudinally polarised ^{3}He target. While the proton and the neutron inside ^{2}H are essentially in s-states of relative motion with aligned spins, ^{3}He is (with $\sim 90\%$ probability) a system consisting of two protons with spins paired off and an active unpaired neutron, in relative s-states. As a result, the spin structure of ^{3}He strongly suppresses the polarisation-dependent proton contribution with respect to the ^{2}H case. This advantage compensate for the more simplicity of the ^{2}H nucleus. Moreover, the combined analysis of measurements using both ^{2}H and ^{3}He targets will play a crucial role in constraining theoretical predictions and in establishing the validity of the models that will be used for the extraction of the GDH integral for the free neutron.

Moreover, the helicity dependence of the $\gamma n \to N\pi$ reactions provides an important testing ground for multipole models. Up to now, estimates of the strength of different multipoles are mostly based on unpolarised single pion photoproduction data, the great majority of which were taken on the proton. However, as clearly demonstrated (see, for instance, [9]), polarisation observables are a much better tool for disentangling the role of the different electromagnetic multipoles due to the change of sign of some contributions and the presence of interference terms between different multipole amplitudes.

An additional interest to this measurement comes from the investigation of the GDH sum rule on the ^{3}He itself. The sum rule predictions for ^{3}He and the neutron, based on the known values of their anomalous magnetic moment, are 496 μb and 233 μb, respectively. Below pion production threshold, ^{3}He photodisintegration processes have then to show about the same positive helicity-dependent difference as pion photoproduction reactions in order to fulfill the GDH constraint.

Theoretical calculations of the GDH contribution below pion production threshold, evaluated using state-of-the-art three-body calculations [10,11], predict a positive value for the helicity-dependent difference but the estimated contributions exhibit a very strong dependence on the details of the current operators, which are still not well known. This feature is not present in the case of the unpolarised observables where, within each calculation, predictions based on different current operators agree. In order to test the basic predictive ability of any model of deuteron or ^{3}He structure, precise experimental data are clearly required from photodisintegration threshold upwards.

The detection system presented in this Letter is not suitable for accessing such low energies. However the data than can be collected, both on the inclusive and on the partial reaction channels, will allow a careful check of the ^{3}He models beyond the π production region. Such a study, when combined with the very recent data close to the break-up threshold region from at the upgraded HIγS facility of the TUNL laboratory (Durham NC, USA) [12], will provide a clean verification of the GDH sum rule on ^{3}He and a much deeper insight into the elementary mechanisms of the γ ^{3}He interactions.

As a first step in this new experimental program, we present in this Letter the first measurement on the helicity-dependent total inclusive photo-absorption cross section on ^{3}He from 200 to 500 MeV together with helicity-dependent measurements for the γ ^{3}He $\to ppn$ reaction and the semi-exclusive γ ^{3}He $\to \pi^0 X$ and γ ^{3}He $\to \pi^{\pm} X$ reactions.

2. Experimental setup

The experiment was carried out at the tagged photon facility of the MAMI accelerator in Mainz. Circularly polarised photons were obtained by bremsstrahlung of longitudinally polarised electrons having an energy of 525 MeV and an average polarisation of about 80% [13]. The relative electron polarisation was continuously monitored using a Moeller polarimeter [14] and its absolute value was periodically measured using a Mott polarimeter [15]. This parameter was then determined with an absolute accuracy of 3%. The bremsstrahlung photons were tagged using the Glasgow–Mainz magnetic spectrometer with an energy resolution of about 1 MeV [16–18]. The relative tagging efficiency was monitored throughout the experiment using an ionisation chamber, which measures the overall bremsstrahlung flux, and absolute measurements were regularly made by a total absorption lead glass detector, which was moved into the beam line at reduced photon intensity. In this way, the intensity of the tagged photon flux was known with an accuracy of 5% [19].

* Corresponding author.
E-mail address: pedroni@pv.infn.it (P. Pedroni).
[1] Present address: University of Massachusetts, Amherst, USA.
[2] Present address: Physics Institute, University of Bonn, Germany.
[3] Present address: IPNL, University of Lyon, France.

A high-pressure ($\simeq 4$ bar) polarised ^{3}He gas target has, for the first time, been used with a photon beam line. The polarised gas was contained in a cylindrical cell with a total length of 20 cm and an outer diameter of 6 cm. The cell is made from quartz glass with two 50 μm thick titanium foils as entry and exit windows for the photon beam. These materials were chosen since they provide the necessary gas tightness and give an acceptably long gas polarisation relaxation time. The gas was polarised outside the experimental area and the target cell was then inserted into the detector system where a solenoid provided a very homogeneous guiding magnetic field to maintain the polarisation alignment. A relative measurement of the polarisation was performed every hour using NMR techniques. The principles of operation for this target, as well as the complete target setup used in the experiment, are detailed in [20]. The ^{3}He nuclei were polarised typically up to about 70% with relaxation times of about 20 hours. The target density and polarisation degree were known with an accuracy of 2% and 5%, respectively [20].

The detector system setup was composed of (1) the Crystal Ball (CB) detector a large solid angle, highly segmented photon and hadron calorimeter, (2) a Particle Identification Detector (PID), (3) the Multi-Wire Proportional Chambers (MWPCs) used to identify and track the charged particles in the CB detector, and (4) a threshold Cherenkov detector.

The CB spectrometer [21] is a sphere consisting of 672 optically isolated NaI(Tl) crystals, shaped as truncated triangular pyramids that point toward the center of the sphere. Each NaI(Tl) crystal is 41 cm long, which corresponds to 15.7 radiation lengths. The crystals are arranged in two hemispheres that cover 93% of 4π sr.

The target was surrounded by the PID [22], which is formed by 24 scintillators and is used to distinguish between neutral and charged particles as well as to discriminate the different types of charged particles detected by the CB. The MWPCs surround the PID and were similar to those originally used as part of the DAPHNE detector [23]. They were used to reconstruct the trajectories of charged particles emitted within the angular and momentum acceptance of the CB detector.

The combined information from these three detectors provided accurate energy, angle, and particle identification in the azimuthal (ϕ) and polar (θ) angle ranges from 0° to 360° and 21° to 159° respectively.

Finally, in order to suppress as much as possible the background originating from reactions on the atomic electrons, a threshold Cherenkov detector was installed. The detector was located downstream of the CB detector to cover the polar angular range from 0° to 18°, where nearly all atomic events occur. The detection of the $e^{\pm}$ coming from pair production or Compton process was used to veto events in which the other particle scatters into the CB detector.

3. Unpolarised data

3.1. Total inclusive cross section

To avoid large systematic uncertainties arising from the detection of all the individual reaction channels, an inclusive method of data analysis was developed to determine the total inclusive photo-absorption cross section σ_{tot} for ^{3}He directly (see, for instance, [24]). In this method the identification of individual processes is not required; what is necessary is to observe at least one reaction product of all possible hadronic final states, with almost complete acceptance, as far as solid angle and efficiency are concerned. The corrections needed to evaluate the detector efficiencies and the loss of events emitted in the angular/momentum regions not covered by the detector have to be kept as low as possible to minimize model-dependent extrapolations. Due to the almost isotropic distributions of the photo-emitted pions and of the protons from photodisintegration in the considered photon energy range, the CB detector, with a very large covered solid angle and an intrinsic detection efficiency $\gtrsim 99\%$ for both charged hadrons and photons coming from neutral meson decays, meets these requirements.

The event selection procedure for the inclusive method was quite simple: at least one cluster signal (i.e., a group of adjacent hit crystals) was required in the CB. However to reject atomic background, only clusters that had a total energy of 40 MeV or higher were used in the analysis. Monte Carlo simulations show that, under these conditions, a large fraction of σ_{tot} (from $\sim 90\%$ at $E_\gamma = 200$ MeV to $\sim 96\%$ at $E_\gamma = 500$ MeV) can be directly accessed since, for the dominant quasi-free processes on single nucleons, the minimum pion momenta for the $\pi^{\pm}X$ channels are above the CB detection threshold.

A model-dependent extrapolation was evaluated to obtain the remaining part of the total photo-absorption cross section, which produces events where all charged hadrons and/or photons from π^0 decays are emitted outside the detector acceptance. Corrections for the $\gamma\ ^3\text{He} \to \pi X$ reactions were evaluated assuming that only quasi-free processes on single nucleons are present and using the angular distributions for the $\gamma N \to \pi N$ processes predicted by the MAID multipole analysis [25]. The missing $\Delta(ppn)$ contribution from the $\gamma\ ^3\text{He} \to ppn$ reaction was evaluated on the assumption that the dominant reaction mechanism is the absorption on a correlated (n, p) pair. The missing contribution $\Delta(ppn)$ of this reaction was then taken to be [24]:

$$\Delta(ppn) = \alpha * \Delta(pn), \tag{2}$$

where the missing contribution $\Delta(pn)$ from the $\gamma\ ^2\text{H} \to pn$ reaction was evaluated using previously published DAPHNE data [26] and the parameter α was taken equal to 1.68 [24].

Monte Carlo simulations show that losses from the $\gamma\ ^3\text{He} \to pd$ reaction and from $\gamma\ ^3\text{He} \to ppn$ due to three-nucleon absorption mechanisms are much less than 1% of the measured total inclusive yield and can be neglected. Due to the very high efficiency ($\gtrsim 98\%$) for the detection of at least one of the two photons coming from the π^0 decay, no correction has been made for the missing part of the coherent $\gamma\ ^3\text{He} \to \pi^0\ ^3\text{He}$ channel.

The systematic uncertainty associated with the simplified models used to evaluate the extrapolation corrections is estimated to be 10% of the calculated correction. The combination of all different sources gives an overall systematic uncertainty of $\sim 5.5\%$ of σ_{tot}.

In Fig. 1a) the values of the unpolarised total inclusive cross section obtained from the present experiment after the subtraction of the empty target spurious contributions are compared to previous results [24]. The good agreement that can be clearly seen with respect to the published measurements gives confidence in the total inclusive procedure.

3.2. Partial reaction channels

In order to provide additional experimental information, the particle identification capabilities of the experimental apparatus were used to evaluate the total cross section for the semi-exclusive processes (i) $\gamma\ ^3\text{He} \to \pi^0 X$ ($\sigma_{\pi^0 X}$), (ii) $\gamma\ ^3\text{He} \to \pi^{\pm} X$ ($\sigma_{\pi^{\pm} X}$), and for the photodisintegration reaction (iii) $\gamma\ ^3\text{He} \to ppn$ (σ_{ppn}). None of these cross sections have been previously measured.

3.2.1. The $\pi^0 X$ channel

The yield from (i) was evaluated by selecting events having two or three neutral clusters in the CB detector. The π^0 mesons

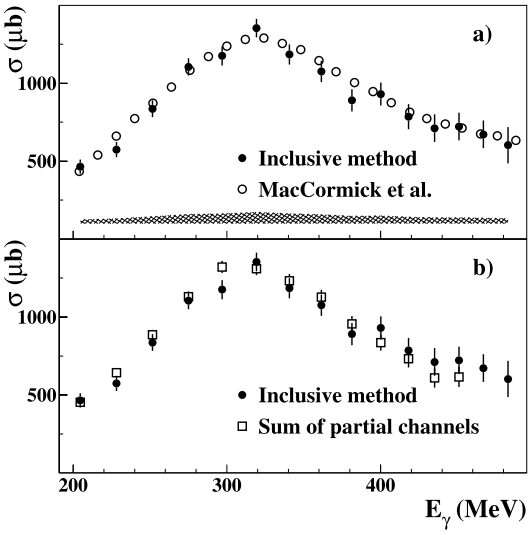

Fig. 1. a) The unpolarised total inclusive cross section on ^{3}He (full circles) is compared to previous results [24] (open circles). The error bars are statistical and the hatched band shows the systematic uncertainties in the present measurement. b) The unpolarised total inclusive cross section on ^{3}He (full circles) is compared to the sum of contributions from the partial reactions channels $\pi^0 X$, $\pi^{\pm} X$ and *ppn*.

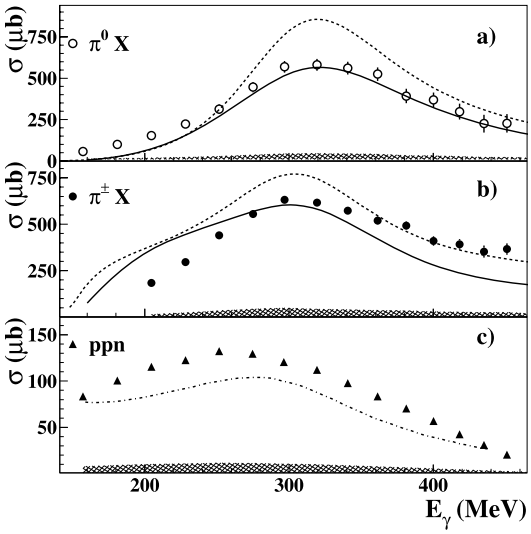

Fig. 2. The unpolarised total cross section for a) $\gamma\ ^3\mathrm{He} \to \pi^0 X$, b) $\gamma\ ^3\mathrm{He} \to \pi^{\pm} X$ and c) $\gamma\ ^3\mathrm{He} \to ppn$. The error bars are statistical and the hatched bands show the systematic uncertainties. In a) and b) the measured cross sections are compared to the FA model (solid line) and to our PWIA model (dashed line) while in c) they are compared to the QD model (dash-dotted line).

were identified by a standard γ–γ invariant mass analysis that has been outlined in [19,27]. The main backgrounds that can contaminate the data are the $\gamma\ ^3\mathrm{He} \to \pi^0\pi^0 X$ reactions. For this reason, the data analysis was limited to $E_\gamma \lesssim 450$ MeV. The small (at most about 5% of the measured yield) contamination present above $E_\gamma \gtrsim 400$ MeV was evaluated assuming the dominance of quasi-free $\gamma N \to \pi^0\pi^0$ processes on single nucleons and using the total unpolarised cross section values for these processes previously measured by the GDH [28–30] and TAPS [31] Collaborations. For this and for the other partial channels, the extrapolation corrections were evaluated as previously explained for the total inclusive method. The systematic uncertainty associated with the event selection procedure and with efficiency corrections was evaluated to be 3% of the measured yield [19]. The addition in quadrature of all the different sources of systematic uncertainties gives an overall systematic uncertainty of about 6% of $\sigma_{\pi^0 X}$.

The results are shown in Table 1 and Fig. 2a), where they are compared to the predictions of the Fix–Arenhövel (FA) model (solid line) and to the predictions (dashed line) of a simple plane-wave impulse approximation (PWIA) model in which the cross sections are evaluated as an incoherent sum of quasi-free single nucleon contributions. The quasi-free nucleon cross sections were determined using the MAID multipole analysis and the momentum distribution of nucleons inside ^{3}He as parameterized in [32]. The FA model is a straightforward extension of the work previously done on the deuteron [33]. The elementary production operator $\gamma N \to \pi N$ is taken from the MAID multipole analysis and is afterwards embedded into the ^{3}He wave function to take into account nuclear effects. Empirical attenuation factors were then applied to take into account the absorption of the photo-emitted particles inside the nuclear medium.

As can be clearly seen from the difference between the two models, the predicted role of the nuclear effects result in damping and broadening the peak corresponding to the Δ resonance excitation. The FA model is in good agreement with our measurements for $E_\gamma \gtrsim 250$ MeV while it underestimates them at lower photon energies, in the region where the coherent $\gamma\ ^3\mathrm{He} \to \pi^0\ ^3\mathrm{He}$ reaction is expected to play a dominant role.

3.2.2. The $\pi^{\pm} X$ and ppn channels

Protons and charged pions hitting the CB were identified by a standard dE/dX vs. E analysis, using the energy information from the CB and PID and the directional information from the MWPCs [19]. In both cases, software cuts on the interaction vertex coordinates of the selected events suppressed most of the events originating from the target walls and windows [20].

The MWPC trajectory reconstruction efficiency was determined using a set of $\pi^{\pm}$ and/or proton events that were unambiguously identified using the approximate dE and E information provided by the PID and CB detectors. These events were related to the MWPC trajectories using the approximate angular information given by the CB detector alone. This efficiency was evaluated by calculating the fraction of such events that have a trajectory reconstructed successfully from the MWPCs information and was found to be $\sim 85\%$ ($\sim 95\%$) for $\pi^{\pm}$ (protons) with a smooth dependence on the incident photon energy. An absolute systematic uncertainty of 3% has been estimated for this parameter.

Events from reaction (ii) were obtained by identifying one charged pion in the CB detector. In a similar way to before, the data analysis was limited to $E_\gamma \lesssim 450$ MeV and the small contamination (at most about 5% of the measured yield) due to $\gamma\ ^3\mathrm{He} \to \pi^+\pi^- X$ processes was evaluated from the $\gamma p \to \pi^+\pi^- p$ cross section measured by the GDH Collaboration [34] and assuming this cross section to be equal to the one for $\gamma n \to \pi^+\pi^- n$ channel. This last assumption is in agreement with the very few published data for this last channel [35].

The systematic uncertainty associated with the event selection procedure and to efficiency corrections was evaluated as 3% of the measured yield. The addition in quadrature of all the different sources of systematic uncertainties gives an overall systematic uncertainty of about 7% of $\sigma_{\pi^{\pm} X}$. The results are shown in Table 1 and Fig. 2b), where they are compared to the predictions of the FA model (continuous line) and of our PWIA model (dashed line). In this case the FA model describes the measured cross sections less well and for $E_\gamma \gtrsim 350$ MeV the simple PWIA model does better.

The yield from reaction (iii) was evaluated by selecting events having one or two protons identified in the CB. Since the major competing background is due to the $\gamma\ ^3\mathrm{He} \to ppn\pi^0$ reaction, the

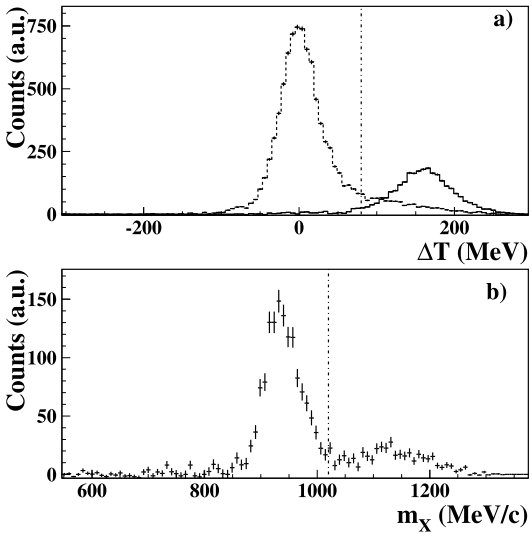

Fig. 3. a) Missing energy (ΔT) distributions for events with one detected proton inside the CB: dashed histogram: events with fewer than two neutral clusters detected in coincidence with the proton; continuous histogram: events with two or more neutral clusters. b) Missing mass (m_X) distribution for events with two detected protons inside the CB. In both cases, the dash-dotted line defines the regions that were taken into account for the *ppn* analysis.

presence of fewer than two neutral clusters detected in the CB, in coincidence with the proton(s) was also required.

The residual background for events having only one detected proton was evaluated taking into account that, in this case, the photodisintegration process is predominantly due to the quasi-deuteron mechanism $\gamma\ {}^3\mathrm{He} \to pnp_{\mathrm{spectator}}$. The measured proton kinetic energy T_{meas} was then compared with the proton kinetic energy T_{calc}, calculated using E_γ and the proton polar emission angle under the assumption the proton originated from the $\gamma\ {}^2\mathrm{H} \to pn$ reaction. The dashed histogram of Fig. 3a) shows the difference $\Delta T = (T_{\mathrm{calc}} - T_{\mathrm{exp}})$ (missing energy) thus obtained. The peak centered near $\Delta T = 0$, smeared by the experimental resolution and the neglect of Fermi motion in the T_{calc} evaluation, is due to *ppn* events, while events from the $ppn\pi^0$ channel show up in the tail at $\Delta T > 0$. This effect can be clearly enhanced when considering the ΔT variable for events having two photons detected in coincidence with the proton, which are (almost) exclusively from the $ppn\pi^0$ channel, as shown by the continuous histogram of Fig. 3a).

For events having two protons in the final state, an analysis of the missing mass for $\gamma\ {}^3\mathrm{He} \to ppX$ was performed. The missing mass is defined as

$$m_X^2 = \left[E_{p_1} + E_{p_2} - (E_\gamma + m)\right]^2 - (\vec{p}_{p_1} + \vec{p}_{p_2} - \vec{p}_\gamma)^2, \qquad (3)$$

where $E_{p_{1,2}}$ ($\vec{p}_{p_{1,2}}$) are the total energies (momenta) of the detected protons, $\vec{p}_\gamma$ is the incident photon momentum, and m is the ^{3}He mass. The experimental m_X distribution, shown in Fig. 3b), shows a peak coming from the *ppn* events and, at higher m_X values, a broad distribution corresponding to the presence of an additional π^0. The two vertical lines in Fig. 3a) and b) define the boundary of the selection zone for *ppn* events. The residual background coming from the $ppn\pi^0$ channel that remained after these cuts was evaluated using the simulation. It was found to be at most a few percent of the total *ppn* yield and was subtracted accordingly. A systematic uncertainty of 5% of the measured yield is estimated in the case for the event selection and efficiency evaluation procedure. The addition in quadrature of all the different sources of systematic uncertainties gives an overall systematic uncertainty of about 8% of σ_{ppn}.

Table 1
The unpolarised total cross section (in μb) for the $\pi^0 X$, $\pi^\pm X$ and *ppn* channels. Both statistical and systematic uncertainties are given.

E_γ (MeV)	$\sigma_{\pi^0 X}$ (μb)	$\sigma_{\pi^\pm X}$ (μb)	σ_{ppn} (μb)
157	$58 \pm 15 \pm 4$		$83 \pm 1 \pm 7$
181	$100 \pm 18 \pm 6$		$101 \pm 2 \pm 8$
205	$154 \pm 21 \pm 9$	$184 \pm 10 \pm 14$	$115 \pm 2 \pm 9$
228	$224 \pm 24 \pm 14$	$297 \pm 13 \pm 23$	$123 \pm 2 \pm 10$
252	$313 \pm 28 \pm 19$	$440 \pm 14 \pm 34$	$132 \pm 2 \pm 11$
275	$446 \pm 31 \pm 27$	$555 \pm 16 \pm 43$	$130 \pm 2 \pm 10$
297	$569 \pm 34 \pm 35$	$631 \pm 18 \pm 49$	$121 \pm 3 \pm 10$
319	$581 \pm 35 \pm 36$	$616 \pm 19 \pm 42$	$112 \pm 3 \pm 9$
341	$561 \pm 38 \pm 35$	$573 \pm 22 \pm 39$	$98 \pm 3 \pm 8$
361	$525 \pm 41 \pm 32$	$520 \pm 23 \pm 36$	$83 \pm 3 \pm 7$
381	$393 \pm 43 \pm 24$	$493 \pm 24 \pm 34$	$71 \pm 3 \pm 6$
400	$369 \pm 44 \pm 23$	$410 \pm 26 \pm 28$	$57 \pm 3 \pm 5$
418	$298 \pm 48 \pm 18$	$391 \pm 28 \pm 27$	$43 \pm 3 \pm 3$
435	$226 \pm 54 \pm 14$	$353 \pm 32 \pm 24$	$31 \pm 3 \pm 2$
451	$228 \pm 56 \pm 14$	$367 \pm 30 \pm 25$	$21 \pm 3 \pm 2$

The two-body break-up channel $\gamma\ {}^3\mathrm{He} \to pd$ was neglected in this analysis due to its very small cross section which, in the measured photon energy range, is at maximum ~ 0.4 μb [36,37] and always less than 1% of σ_{ppn}.

The resulting total unpolarised cross section is shown in Table 1 and Fig. 2c). In this case, since no specific model is available, we compared our data to the predictions of the quasi-deuteron (QD) model (see Eq. (2)) with the *pn* contribution on the deuteron taken from the Schwamb–Arenhövel (SA) model [38–40]. As expected, the QD model underestimates our data due to the presence of three-nucleon absorption mechanisms (see, for instance, [41]).

Finally, as a cross-check of all the procedures used in the analysis of the different channels, we compare in Fig. 1b) the total inclusive cross section obtained by adding the $\pi^0 X$, $\pi^\pm X$ and the *ppn* partial cross sections, the only relevant ones in the measured energy range, to the cross section obtained using the inclusive method. The good agreement between the two different sets of points gives further confidence in all these procedures.

4. Polarised data

In the analysis of the helicity-dependent data, all previously mentioned analysis methods were used to evaluate the difference $\Delta\sigma = (\sigma_{\mathrm{p}} - \sigma_{\mathrm{a}})$. In this case the contributions from all unpolarised materials present in the target cell vanish. In a similar way as before, the extrapolation correction for $\gamma\ {}^3\mathrm{He} \to \pi X$ was evaluated using the MAID predictions while the $\Delta(pn)$ contribution was calculated using the predictions of the SA model. The procedure described above results in the polarised total inclusive photoabsorption cross section difference $\Delta\sigma_{\mathrm{tot}}$ as shown in Table 2 and in Fig. 4a) compared with the predictions of our PWIA model. In this case also the effects on the nucleon spin alignments due to the ^{3}He s' and d-state probabilities were taken into account according to the formula [42]:

$$\Delta\sigma_{\mathrm{PWIA}} = p_{\mathrm{n}} \cdot \Delta\sigma_{\mathrm{neutron}} + 2 \cdot p_{\mathrm{p}} \cdot \Delta\sigma_{\mathrm{proton}}, \qquad (4)$$

where $p_{\mathrm{n}} = 0.865$ and $p_p = -0.027$ are the effective degrees of neutron and proton polarisation inside ^{3}He as evaluated by [43] and $\Delta\sigma_{\mathrm{proton\,(neutron)}}$ are the free nucleon polarised cross section differences obtained from MAID and smeared out by the nucleon momentum distribution inside ^{3}He. The agreement between our data and the PWIA model is reasonable, taking into account the non-negligible statistical experimental uncertainties. This is a hint that nuclear effects are less important than in the unpolarised case.

Fig. 4b) shows the dependence of the experimental running integral

Table 2
The polarised total cross section difference $\Delta\sigma$ (in μb) for the total inclusive photo-absorption channel an the $\pi^0 X$, $\pi^{\pm} X$ and *ppn* channels. Both statistical and systematic uncertainties are given.

E_γ (MeV)	$\Delta\sigma_{\rm tot}$ (μb)	E_γ (MeV)	$\Delta\sigma_{\pi^0 X}$ (μb)	$\Delta\sigma_{\pi^{\pm} X}$ (μb)	$\Delta\sigma_{ppn}$ (μb)
211	$-45\pm61\pm7$	157	$7\pm15\pm1$		$147\pm15\pm13$
246	$224\pm61\pm18$	181	$32\pm18\pm3$		$150\pm13\pm13$
281	$392\pm61\pm31$	205	$64\pm21\pm5$	$-143\pm12\pm13$	$147\pm13\pm13$
315	$316\pm61\pm25$	228	$97\pm24\pm8$	$-106\pm13\pm9$	$176\pm13\pm15$
346	$233\pm60\pm19$	252	$185\pm28\pm16$	$-43\pm14\pm4$	$163\pm13\pm14$
376	$248\pm69\pm20$	275	$176\pm31\pm15$	$39\pm14\pm3$	$178\pm12\pm15$
405	$19\pm63\pm2$	297	$230\pm34\pm20$	$54\pm14\pm4$	$145\pm13\pm12$
431	$-96\pm71\pm8$	319	$153\pm35\pm13$	$87\pm13\pm6$	$131\pm10\pm11$
455	$-112\pm70\pm9$	341	$172\pm38\pm15$	$24\pm14\pm3$	$112\pm10\pm9$
479	$-12\pm85\pm2$	361	$159\pm41\pm14$	$-10\pm14\pm3$	$93\pm10\pm8$
		381	$140\pm43\pm12$	$-21\pm14\pm3$	$88\pm10\pm8$
		400	$85\pm44\pm7$	$-69\pm14\pm5$	$60\pm9\pm5$
		418	$80\pm48\pm7$	$-58\pm14\pm5$	$70\pm10\pm6$
		435	$57\pm54\pm5$	$-60\pm16\pm5$	$48\pm10\pm4$
		451	$85\pm56\pm7$	$-23\pm16\pm2$	$31\pm10\pm3$

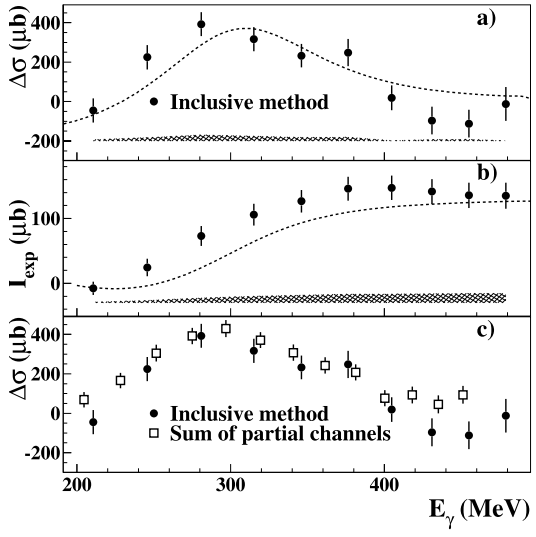

Fig. 4. a) The polarised total inclusive photo-absorption cross section difference on ^{3}He ($\Delta\sigma_{\rm tot}$) (full circles) compared to the predictions of our PWIA model (dashed line). b) The running GDH integral for ^{3}He obtained with the present data compared to the predictions of our PWIA model (dashed line). c) The polarised total inclusive photo-absorption cross section difference on ^{3}He ($\Delta\sigma_{\rm tot}$) (full circles) is compared to the sum of contributions from the partial reaction channels $\pi^0 X$, $\pi^{\pm} X$ and *ppn*. In all plots, the error bars are statistical and the hatched bands show the systematic uncertainties.

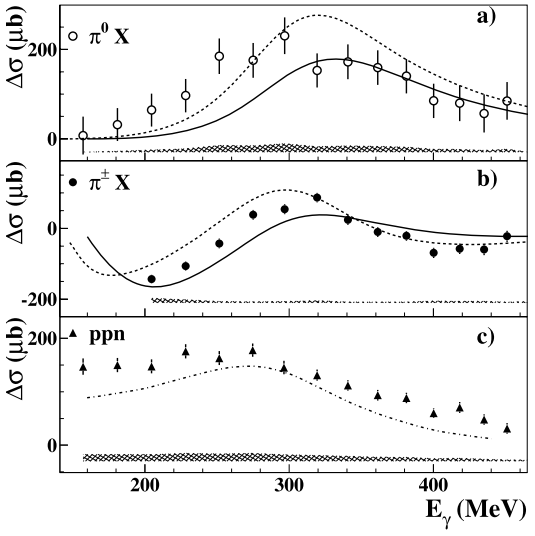

Fig. 5. The polarised total cross section difference $\Delta\sigma$ for the a) γ ^{3}He $\to \pi^0 X$, b) γ ^{3}He $\to \pi^{\pm} X$ and c) γ ^{3}He $\to$ *ppn* reactions. The error bars are statistical and the hatched bands show the systematic uncertainties. In a) and b) the experimental data are compared to the FA model (solid line) and to our PWIA model (dashed line) while in c) they are compared to the QD model (dash-dotted line).

$$I_{\rm exp} = \int_{\nu_0}^{E_\gamma} \frac{\Delta\sigma}{\nu}\, d\nu \tag{5}$$

on the upper integration limit E_γ where ν_0 is the lowest measured photon energy value (200 MeV). The value of $I_{\rm exp}$ for ^{3}He between 200 and 500 MeV amounts to 135 ± 20 (stat) ±12 (sys) μb, which again is in reasonable agreement with the predictions given by our PWIA model. Taking into account that the ^{3}He internal dynamics should reduce the nucleon polarisation compared to the free case by about 20% (see Eq. (4)), the value of the GDH integral for the free neutron should be, as expected, of the same order of magnitude as that for the proton, which, in the same energy range, is equal to 176 ± 8 (stat) ±11 (sys) μb [44].

The polarised cross section difference $\Delta\sigma$ for the (a) $\pi^0 X$, (b) $\pi^{\pm} X$ and (c) *ppn* channels is shown in Table 2 and in Fig. 5 together with the corresponding predictions of the FA model (solid line) and the PWIA model (dashed line) or (for (c)) of the QD model. As in the unpolarised case the FA model only describes the γ ^{3}He $\to \pi^0 X$ measurement at higher photon energies and it does not reproduce the shape of the measured γ ^{3}He $\to \pi^{\pm} X$ data. Our PWIA model reproduces the data at higher photon energies for both reactions reasonably well. This is further confirmation that the effects more directly related to the composite nuclear target structure do not have a strong helicity dependence and their net effect is reduced in the $\Delta\sigma$ case.

The measured $\Delta\sigma$ for the *ppn* channel is higher than the predictions of the QD model. This is a hint that the three-nucleon absorption mechanisms mainly contribute to $\sigma_{\rm p}$.

As before, we compare in Fig. 4c) the helicity-dependent total inclusive photo-absorption cross section obtained by adding the $\pi^0 X$, $\pi^{\pm} X$ and the *ppn* partial channels with the one obtained using the inclusive method. Also in this case, the good agreement, except for the highest energies, between the two different sets of points gives confidence in the different analyses.

5. Conclusions

The helicity dependence of the total inclusive photo-absorption cross section on ^{3}He and both the unpolarised and the helicity-dependent partial cross sections for the reactions $\gamma\ ^3\mathrm{He} \to ppn$, $\gamma\ ^3\mathrm{He} \to \pi^0 X$ and $\gamma\ ^3\mathrm{He} \to \pi^\pm X$ have been measured for the first time at MAMI (Mainz) in the energy region $200 < E_\gamma < 500$ MeV. All these new data provide a very powerful tool to improve further the models for photoreactions on ^{3}He in the Δ resonance region.

Available state-of-the-art calculations are unable to describe in a satisfactory manner both the unpolarised and the helicity-dependent cross section for the πX channels.

A simple PWIA model well reproduces both the unpolarised and the helicity-dependent $\pi^\pm X$ data for $E_\gamma \gtrsim 350$ MeV while the agreement is poorer for the $\pi^0 X$ case. This is a clear hint that for the $\pi^\pm X$ channel nuclear effects play a leading role only in the vicinity of the pion production threshold. For both channels, these effects are shown to be more important in the unpolarised case.

No model is at present available for the ppn channel. A simple quasi-deuteron approach does not fully reproduces the photodisintegration data and the three-nucleon absorption mechanisms should then be taken into account. All previous considerations strongly motivate further theoretical and experimental research in the field. In order to pin down the origin of the observed discrepancies, an analysis of both the unpolarised and polarised differential cross sections for the $\gamma\ ^3\mathrm{He} \to \pi^0 X$ and $\gamma\ ^3\mathrm{He} \to \pi^\pm X$ reactions is underway. These results will be the subject of a future publication.

Acknowledgements

The authors wish to acknowledge the excellent support of the accelerator group of MAMI. This work was supported by the Deutsche Forschungsgemeinschaft (SFB 443), the INFN–Italy, the European Community-Research Infrastructure Activity under the FP7 programme (Hadron Physics2, grant agreement No. 227431), the UK STFC research council, the Natural Science and Engineering Research Council (NSERC) in Canada, the National Science Foundation and Department of Energy in the United States, and the RF Federal program “Kadry” (contract number 14.B37.21.0786). W.J.B. acknowledges the support of U.S. Department of Energy Grant No. DE-FG02-99ER41110.

References

[1] S. Gerasimov, Sov. J. Nucl. Phys. 2 (1966) 430.
[2] S. Drell, A. Hearn, Phys. Rev. Lett. 16 (1966) 908.
[3] J. Ahrens, et al., Phys. Rev. Lett. 87 (2001) 022003.
[4] H. Dutz, et al., Phys. Rev. Lett. 91 (2003) 192001.
[5] H. Dutz, et al., Phys. Rev. Lett. 93 (2004) 032003.
[6] H. Dutz, et al., Phys. Rev. Lett. 94 (2005) 162001.
[7] J. Ahrens, et al., Phys. Rev. Lett. 97 (2006) 202303.
[8] J. Ahrens, et al., Phys. Lett. B 672 (2009) 328.
[9] J. Ahrens, et al., Phys. Rev. Lett. 88 (2002) 232002.
[10] A. Detulva, et al., Phys. Rev. C 69 (2004) 034004.
[11] J. Golak, et al., Phys. Rev. C 74 (2005) 044002, arXiv:1304.5442, 2013.
[12] G. Laskaris, et al., arXiv:1304.5442 [nucl-ex], 2013.
[13] K. Aulenbacher, et al., Nucl. Instrum. Methods A 391 (1997) 498.
[14] I. Preobajenski, PhD thesis, University of Mainz, 2001.
[15] V. Tioukine, K. Aulenbacher, N. Riehn, Rev. Sci. Instrum. 82 (2011) 033303.
[16] I. Anthony, et al., Nucl. Instrum. Methods A 301 (1991) 230.
[17] S.J. Hall, et al., Nucl. Instrum. Methods A 368 (1996) 698.
[18] J. McGeorge, et al., Eur. Phys. J. A 37 (2008) 129.
[19] S. Schuman, et al., Eur. Phys. J. A 43 (2010) 269.
[20] J. Krimmer, et al., Nucl. Instrum. Methods A 648 (2011) 35.
[21] A. Starostin, et al., Phys. Rev. C 64 (2001) 055205.
[22] D. Watts, in: Calorimetry in Particle Physics: Proceedings of the 11th International Conference, World Scientific, Singapore, 2005, p. 560.
[23] G. Audit, et al., Nucl. Instrum. Methods A 301 (1991) 473.
[24] M. MacCormick, et al., Phys. Rev. C 53 (1996) 41.
[25] D. Drechsel, S. Kamalov, L. Tiator, Eur. Phys. J. A 34 (2007) 69.
[26] R. Crawford, et al., Nucl. Phys. A 603 (1996) 303.
[27] C. Tarbert, et al., Phys. Rev. Lett. 100 (2008) 132301.
[28] J. Ahrens, et al., Phys. Lett. B 551 (2003) 49.
[29] J. Ahrens, et al., Phys. Lett. B 624 (2005) 173.
[30] J. Ahrens, et al., Eur. Phys. J. A 47 (2011) 36.
[31] M. Kotulla, et al., Phys. Lett. B 578 (2007) 63.
[32] R. Schiavilla, V. Pandharipande, Nucl. Phys. A 449 (1986) 219.
[33] H. Arenhövel, A. Fix, Phys. Rev. C 72 (2005) 064004.
[34] J. Ahrens, et al., Eur. Phys. J. A 34 (2007) 11.
[35] F. Carbonara, et al., Nuovo Cimento 36A (1976) 219.
[36] H. Gassen, et al., Zeit. Phys. A 303 (1981) 35.
[37] V. Isbert, et al., Nucl. Phys. A 578 (1994) 525.
[38] H. Arenhoevel, M. Schwamb, Nucl. Phys. A 690 (2001) 647.
[39] H. Arenhoevel, M. Schwamb, Nucl. Phys. A 690 (2001) 682.
[40] H. Arenhoevel, M. Schwamb, Nucl. Phys. A 696 (2001) 556.
[41] G. Audit, et al., Nucl. Phys. A 614 (1997) 461.
[42] C. Ciofi degli Atti, S. Scopetta, Phys. Lett. B 404 (1997) 223.
[43] J. Friar, et al., Phys. Rev. C 42 (1990) 2310.
[44] J. Ahrens, et al., Phys. Rev. Lett. 84 (2000) 5950.